http://journal.uir.ac.id/index.php/JGEET

E-ISSN : 2541-5794
P-ISSN : 2503-216X

Journal of Geoscience,
Engineering, Environment, and Technology
Vol 11 No 3 2026

RESEARCH ARTICLE

Screening-Level Liquefaction Susceptibility Assessment in Central West Lombok: Integrating HVSR-Derived Ground Shear Strain and Groundwater Depth

Ilham [1]*, Nevi Ernita [1], Ichwan Arief Ramdhani [1], Lalu Aldi Pranata [1]

[1] *Physics Education department, Faculty of Education and Teacher Training, Universitas Islam Negeri Mataram, Mataram City, Indonesia.*

* Corresponding author : ilham.fisika@uinmataram.ac.id
Tel.:+6812-2618-5211
Received: Feb 18, 2026; Accepted: Jul 20, 2026.
DOI: 10.25299/jgeet.2026.11.3.27334

Abstract

Lombok is one of the earthquake-prone areas in Indonesia that is highly exposed to secondary hazards such as liquefaction. This research presents a screening-level liquefaction susceptibility assessment for the central part of West Lombok by integrating two main controlling parameters, namely ground shear strain (GSS) derived from HVSR microtremor measurements (n = 52) as an indicator of surface soil deformability, and groundwater depth (GWD) from field observations as an indicator of soil saturation level. The Liquefaction Susceptibility Index (LSI) was calculated by combining these two parameters using an unweighted conjunctive geometric mean approach to emphasize the simultaneous occurrence of soil deformability and groundwater saturation conditions while reducing compensatory effects that may occur in additive integration methods. The idea behind this approach is that locations where both high soil deformability and shallow groundwater levels are present will be assigned higher susceptibility values, while the susceptibility values will be reduced for locations where these two prerequisites are mismatched. The integrated LSI offers a more selective zonation than the single parameter outputs: the GWD-only map identifies widespread hydrologically favorable conditions (77.24% are classified as High–Very High) as saturation-ready, and the GSS-only map is dominated by Moderate–Low deformability (73.51%). The integrated map classifies 34.79% of the study area as High, 55.40% as Moderate and 9.80% as Low, with no Very High class. High susceptibility is concentrated in the western coastal belt (Labuapi–Gerung–Lembar), which corresponds to low-lying coastal/alluvial plains underlain by Quaternary alluvium where shallow groundwater and mechanically susceptible ground are more likely to coincide. However, the proposed susceptibility model has not been validated using CPT/SPT measurements, borehole observations, or documented liquefaction inventories. Therefore, the resulting map should be interpreted as a proxy-based screening-level prioritization tool for guiding future geotechnical investigations rather than a deterministic assessment of liquefaction occurrence.

Keywords: Ground Shear Strain, Groundwater Depth, Liquefaction, Microzonation

1. Introduction

Indonesia is located on the Sunda-Banda arc, where many active tectonic plates converge and the fast plate convergence and complex faulting lead to frequent damaging earthquakes and strong site effects in the sediment-filled basins (Hutchings & Mooney, 2021). The Flores Back-Arc Thrust system is one of the several seismogenic sources affecting the Province of West Nusa Tenggara including Lombok Island (Irsyam et al., 2017). The mainshock of August 5, 2018 in Lombok (Mw 6.9) and its aftershocks had a substantial impact on the whole island with widespread damage to buildings and increased population exposure to threats of ground failure (Pebrianto & Hidayat, 2018; USGS, 2018). These instances suggest that the earthquake risk in Lombok is not only attributable to the shaking strength but also to the spatially confined secondary ground failures. Therefore, early diagnosis of susceptibility for soil breakdown at planning scale is crucial to enable risk mitigation based development in quickly developing locations.

Liquefaction is one of the most devastating forms of earthquake-induced soil failure, because it can suddenly reduce the effective stress and shear strength of water-saturated loose granular sediments. This may cause differential settling, lateral spreading and loss of soil bearing capacity (Bao et al., 2019; Towhata, 2008). After the great Alaska and Niigata disasters of 1964, a basic evaluation framework for liquefaction potential assessment started to be developed on the basis of many case studies throughout the world and it is still extensively used in engineering practice and has been refined continually up to now (Youd et al., 2001). Liquefaction phenomena have been observed in Indonesia in several major earthquakes such as the 2006 Yogyakarta earthquake and 2018 Palu earthquake, where liquefaction-induced soil deformation significantly contributed to the damage in urban areas (Sarah & Soebowo, 2013; Soebowo et al., 2007; Upomo et al., 2024). A similar observation was obtained for the 2018 Lombok earthquake sequence (Supartoyo et al., 2020), which emphasizes the importance of systematic liquefaction susceptibility mapping as a macro-scale screening tool to assist mitigation efforts and land-use decision making in quickly growing locations. Here, term "susceptibility" is used in the sense of relative zoning on the basis of proxy parameters and not in the sense of deterministic evaluation of liquefaction trigger such as CSR–CRR safety factor.

There are two main factors associated with each other to choose the center part of West Lombok as the main area for this study. The first cause is the geological one where the area is covered by huge youthful deposits such as alluvial plains and other loose materials which are highly sensitive to liquefaction when they are saturated (Mangga et al., 1994). The regional geological mapping and the subsequent investigations have also pointed out the role of the surface materials of the Quaternary age in determining the surface seismic response and the associated geohazards on Lombok Island (Rachmat et al., 2016). Secondly, from the perspective of regional planning, this area is designated as part of the West Lombok-Mataram strategic growth corridor in the 2024-2044 West Nusa Tenggara Provincial Spatial Plan (RTRW) (Pemerintah NTB, 2024), so that the level of exposure to geological hazards is expected to continue to increase. Liquefaction susceptibility mapping is, in this sense, not only of academic significance but also a significant input for spatial planning, prioritization of infrastructure development and catastrophe risk reduction measures. This is especially so when land-use changes are occurring at a faster rate than the availability of accurate and appropriate subsurface geotechnical data.

The liquefaction potential is usually evaluated from field and laboratory geotechnical data (e.g. SPT/CPT) to obtain parameters such as the cyclic resistance ratio and factor of safety by employing common methodologies and their developments (Hatmoko & Suryadharma, 2015; Mustafa et al., 2025). These are the most direct means to characterize subsurface conditions; yet, their use is generally limited by cost, logistics and spatial coverage. Constraints are more applicable to mapping at a regional scale, especially for areas lacking a clear network of drilling data. Consequently, regional liquefaction susceptibility assessments frequently incorporate geophysical and subsurface proxy information to complement sparse geotechnical observations (Aditama et al., 2021). This stimulates the employment of more efficient and non-destructive alternative methodologies such as the microtremor analysis using Horizontal-to-Vertical Spectral Ratio (HVSR) method (Nakamura, 2019).

The Nakamura-type formulations are produced from the HVSR outputs, which define the vulnerability index (Kg) from the resonance frequency and the amplification peak that can be used to assess the ground shear strain (GSS) as a first-order indicator for the potential for large deformation during strong shaking (Ilham et al., 2021; Kurniawan et al., 2023; Kusuma & Sanny, 2022; Manan et al., 2023; Yatini et al., 2023). Kg/GSS mapping has thus been utilized as a screening layer at planning scale to locate locations prone to non-linear near-surface response and localized deformation where dense geotechnical datasets are missing (Alonso-Pandavenes et al., 2024). In this sense, GSS is seen as an indirect index for liquefaction triggering, as a proxy for deformability (mechanical susceptibility). Similar HVSR-based approaches have been successfully applied in several Indonesian settings to characterize seismic site response, soft sediment distribution, and deformation susceptibility (Mulyana et al., 2026; Prabowo et al., 2021).

However, liquefaction requires by definition two conditions: an adequate cyclic demand imposed by earthquake shaking and a susceptible (usually saturated or near-saturated) soil state with a reduction in effective stress and strength due to excess pore water pressure (Youd et al., 2001). Using only proxy parameters of shaking/deformation (e.g., GSS) for susceptibility mapping may exaggerate hazard in places where the soil is not saturated since the depth-to-groundwater strongly controls the effective stress in the soil. Conversely, mapping by depth of groundwater alone can overestimate areas with high site responsiveness and seismic deformation needs (Chung & Rogers, 2013). The post-disaster analysis of the 2018 Palu earthquake revealed that groundwater depth is a major determinant in generating liquefaction besides soft sediment thickness and HVSR based site reaction (Jalil et al., 2021). Several studies of microtremor/HVSR in Lombok have proven that the metrics acquired from HVSR are beneficial to identify liquefaction prone zones. However, groundwater level data are usually presented as supporting background rather than included into fully replicable quantitative models (Taruna et al., 2024). This constraint is particularly important to central West Lombok where there is considerable hydrogeological heterogeneity and geographical variance in surface sediment reaction. Therefore, a liquefaction susceptibility screening approach is needed that simultaneously considers seismic deformation demand and groundwater-controlled soil saturation. Because liquefaction requires the concurrence of these conditions, a non-compensatory integration rule is adopted to reduce false positives where only one prerequisite is present.

To satisfy this need in a transparent and repeatable method, in the present study, the HVSR-based GSS values and the groundwater depth (GWD) are standardized into equivalent susceptibility scores and then combined by the operator of conjunctive geometric mean without weights. This integration strategy is conjunctive and has a limited compensation in the sense that susceptibility levels dramatically increase only when two proxy factors are simultaneously high. On the other hand, the disparity between the high and low characteristics will be demoted (usually to the moderate class) and not directly classed as high. The maps developed in this study are meant as planning level screening output to indicate priorities for further extensive site inquiry and are not intended to replace Factor of Safety (FS) based liquefaction trigger analysis utilizing SPT/CPT data.

Therefore, this study constructs a screening-level liquefaction susceptibility model for the central West Lombok region by combining GSS obtained from microtremor analysis as a proxy of seismic deformation demand and GWD as a proxy of soil saturation readiness level. The main contributions of this study are (1) the use of a simple, reproducible and mechanistically consistent integration method through a conjunctive approach (geometric mean and rule-based interaction matrix) that could be used for regional filtering in data-limited areas; and (2) the evaluation of three mapping scenarios, i.e. GSS-based only, GWD-based only and GSS–GWD integration to show how single-parameter-based approaches could produce less accurate representations of susceptibility patterns whereas the integration of the two approaches could lead to more reliable zoning to support hazard mitigation-based spatial planning in central West Lombok.

Several multi-criteria integration techniques have been widely applied in susceptibility mapping, including weighted overlay, fuzzy logic, and Analytical Hierarchy Process (AHP). Most of these approaches allow varying degrees of compensatory behaviour, whereby a high score in one variable may offset a low score in another. However, liquefaction is fundamentally controlled by the simultaneous occurrence of multiple prerequisite conditions, particularly soil deformability and sufficient

saturation. For this reason, a conjunctive geometric mean approach was adopted because it behaves as a non-compensatory integration method, reducing susceptibility values when one of the controlling factors is weak even if the other is high. This characteristic better reflects the physical requirements of liquefaction occurrence than additive integration schemes. Equal weighting was assigned to both variables because no independent geotechnical dataset was available to objectively calibrate their relative importance. Although this assumption may introduce some bias, it avoids subjective weighting and provides a transparent and reproducible framework for regional-scale screening assessments.

2. Regional Geology

Lombok island is located in the volcanic arc of Sunda-Banda that is formed by the subduction of the Indo-Australian Plate beneath the Eurasian Plate. The regional tectonic setting is controlled by active subduction to the south of Lombok and back-arc compression to the north represented by the Flores Back-arc Thrust system (Simandjuntak, 2014). The Flores Back-arc Thrust has been identified as the principal source of the 2018 Lombok earthquake sequence and contributes significantly to the high seismicity of the region (Sasmi et al., 2020). This seismic setting is relevant to liquefaction susceptibility because strong ground shaking is a primary triggering factor for liquefaction.

The morphology of Lombok Island is dominated by volcanic landforms. The major lithology comprises volcanic rocks, including lava, volcanic breccia, lapilli, tuff and pumice. The general topography of the island consists of three primary groups, including lowlands, volcanic units and undulating to steep hills (Supartoyo et al., 2018). Lowland plains are mainly distributed along the coastal areas, including Mataram City and the central part of West Lombok, and are characterized by gentle topographic gradients. These lowland areas are predominantly underlain by Quaternary alluvial and coastal deposits consisting of sand, silt, clay, and young volcanic materials. Such unconsolidated sediments generally exhibit lower stiffness, higher groundwater storage capacity, and stronger seismic amplification compared with the surrounding volcanic uplands. Consequently, they provide geological conditions favorable for both elevated ground shear strain (GSS) and shallow groundwater depth (GWD), two key prerequisites considered in this study.

Based on the geological map of the Lombok Sheet (Figure 1), the rock units in the study area of central West Lombok are grouped into six major formations from the youngest to the oldest, namely (1) Alluvium (Qa) composed of gravel, sand, clay, coral fragments, and peat, (2) Kalibabak Formation (TQb) composed of breccia and lava, (3) Kalipalung Formation (TQp) composed of alternating marl breccia and lava, (4) Pengulung Formation (Tomp) composed of breccia, lava, and tuff with limestone inserts, (5) Kawangan Formation (Tomk) composed of alternating quartz sandstone, claystone, and breccia, and (6) Intrusive Rocks (Tmi) composed of dacite and basalt. On the map (Figure 1), the main unit in the study area is the Alluvium unit (Qa). These Quaternary alluvial deposits are generally characterized by loose packing, weak consolidation, and high porosity, conditions that favor seismic amplification and cyclic ground deformation during strong earthquake shaking (Loviknes et al., 2024; van Ginkel et al., 2022).

The western lowlands of Lombok are hydrogeologically part of the Mataram-Selong groundwater basin . The area has prolific unconfined aquifers in Quaternary alluvial and volcaniclastic deposits (Syafaat et al., 2024). The presence of sand-rich alluvium and reworked pumice-bearing layers supports the capacity of these deposits to retain and transfer groundwater (Malawani et al., 2024). Moreover, the presence of thick sandy sediment layers with a very shallow groundwater table up to less than 2 meters in many places have been proven by previous geophysical research (Sudrajat et al., 2026). These hydrogeological conditions promote high levels of soil saturation and may increase liquefaction susceptibility during strong seismic shaking.

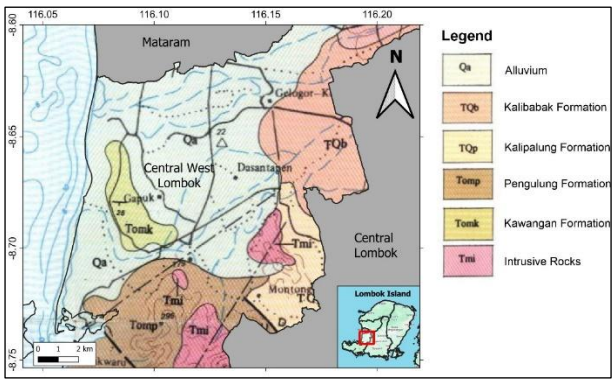

Fig. 1 Geological map of the study area in central West Lombok. The most dominant formation in the research region is Alluvium (Qa) (adapted from Mangga et al. (1994))

Collectively, the geological and hydrogeological characteristics of central West Lombok provide favorable conditions for liquefaction development. The presence of unconsolidated Quaternary alluvial deposits is likely to cause seismic amplification and ground deformation during strong earthquake shaking, while the productive shallow aquifer system leads to high levels of soil saturation in the lowland areas. The conditions are expected to favor spatial coincidence of high GSS and shallow GWD values with respect to the adjacent volcanic and bedrock-dominated areas. In this context, ground shear strain (GSS) is used as a proxy for the seismic deformation demand and groundwater depth (GWD) is used as a proxy for the degree of saturation readiness. Hence, combining these parameters yields a screening-level framework for identifying where mechanical and hydrological prerequisites for liquefaction are most likely to coincide.

3. Data and Methods

3.1 Study Area and Data Collection

This research was conducted in West Lombok Central Region, Indonesia (8.631649°-8.726684° S and 116.062876°-116.1877546° E) . The main data used are single station microtremor recordings and groundwater depth (GWD) measurements obtained at 52 observation points (Figure 2). The sampling locations were selected using a purposive strategy to ensure representation of the principal geological, geomorphological, and hydrogeological settings across the study area, including coastal plains, alluvial deposits, inland areas, and different groundwater conditions. The objective was not to achieve statistical representativeness but to capture the dominant environmental variability relevant to liquefaction susceptibility assessment. Nevertheless, purposive sampling may introduce spatial bias because observation points are not distributed randomly. Consequently, the resulting maps should be interpreted as regional-scale screening products rather than site-specific assessments.

We recorded microtremor data using a DS-4A (0.5–50 Hz) seismometer connected to a TDL 303S digital portable seismograph with a GPS. The recordings were made in accordance with the SESAME (2004) guidelines for 40 min per station at a sampling rate of 100 Hz ensuring a firm coupling to the ground and documenting transient disturbances. In open, private wells close to the microtremor stations, manual measurements of the depth to groundwater were carried out. Groundwater depth was measured as the vertical distance from the local ground surface at each observation point to the observed static water level within the well. Therefore, the measurements represent groundwater depth relative to the surrounding land surface rather than absolute groundwater elevation, minimizing the influence of local topographic differences on susceptibility classification. Measurements were taken in August 2025, which coincides with the local dry-season period. Rainfall during the campaign was intermittent, however, water levels recorded during the campaign are representative of dry season conditions with episodic recharge. Because the measurements were obtained during a single field campaign, the recorded groundwater depths should be interpreted as a temporal snapshot rather than long-term average groundwater conditions. Seasonal groundwater fluctuations may modify groundwater depth classes, particularly near classification boundaries, and therefore constitute an additional source of uncertainty in the susceptibility assessment. Episodic recharge is accounted for in the interpretation as a source of temporal uncertainty.

3.2 Data Processing

Ambient vibration recordings were processed with the software Geopsy (Wathelet et al., 2020) to compute horizontal-to-vertical spectral ratios (HVSR) according to a standardized workflow: selection of stable windows (30s), window tapering with a 0.5% Tukey function, and spectral smoothing with the Konno & Ohmachi algorithm with a smoothing constant of 40 (Cox et al., 2020; Konno & Ohmachi, 1998). The average HVSR curves obtained were assessed for clarity and reliability using the SESAME criteria, assisted by MicroHVSR Control software (Ilham & Sani, 2025), to ensure that the peaks of the resulting curve were stable and well interpretable. For each HVSR curve that met the criteria, the dominant frequency f_0 (Hz) and the peak amplification A_0 (dimensionless) were extracted. Then, the seismic vulnerability indeks K_g was computed as follows using these parameters:

$$K_g = \frac{A_0^2}{f_0} \tag{1}$$

The bedrock peak ground acceleration (PGA) for each site was estimated using the Fukushima et al. (2002) attenuation relationship (Eq. 2). This model had the smallest mean percentage error compared to other empirical PGA models (Saputri & Pujiastuti, 2020), which was verified locally using accelerograph observation from the Mataram station.

$$log\ \alpha = 0.42M_w - log(R + 0.025 \cdot 10^{0.42M_w}) - 0.0033R + 1.22 - 0.14L \tag{2}$$

where α is the average maximum horizontal acceleration (PGA, cm/s^2), M_w is the moment magnitude, R is the hypocentral distance (km), and L is a dummy variable. For this study, $L = 1$ was used, as specified for regions outside Japan. The site-specific PGA value was defined as the maximum PGA from all evaluated events for that site (mainshock and major aftershocks of the 2018 Lombok sequence), representing a conservative, scenario-based estimate of shaking demand during the 2018 Lombok earthquake sequence. The "maximum-over-events" approach mitigates underestimation due to event-to-event variability of the 2018 sequence and provides an upper-bound shaking demand appropriate for planning-scale susceptibility screening.

The ground shear strain (GSS, γ) is considered a deformation-demand proxy (screening indicator) during the analysis and not a substitute for factor-of-safety triggering calculations based on SPT / CPT. GSS was computed by combining local site response and regional bedrock PGA using Nakamura's formulation (Nakamura, 2008),

$$\gamma = K_g \times \alpha \times 10^{-6} \tag{3}$$

Point-based GWD and GSS data were interpolated using ordinary point kriging after all coordinates were converted into UTM units. Experimental variograms were constructed using an omnidirectional setting with direction = 0° and tolerance = 90°. Because the dataset consisted of 52 observation points, six lag classes were used to reduce instability in the experimental variogram. Linear, spherical, and exponential variogram models were tested for each variable. Model selection was based on visual agreement with the experimental variogram, cross-validation performance, and the ability of the resulting grid to preserve the range required for susceptibility classification.

Cross-validation was performed using all 52 observation points. Interpolation performance was evaluated using mean error (ME), mean absolute error (MAE), and root mean square error (RMSE). Prediction uncertainty was assessed using kriging standard deviation grids generated from the selected final models. The influence of observation density was evaluated using nearest-neighbor spacing and the number of data points used during kriging validation.

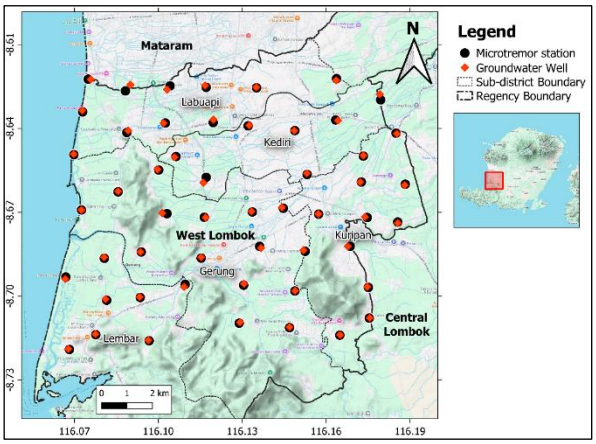

Fig. 2 Distribution of the measurement points: microtremor stations (black circles) and groundwater wells (red squares) (n = 52 locations)

3.3 Integration Model and Classification

Liquefaction susceptibility was modelled by integrating (i) seismic deformation demand represented by ground shear strain (GSS, γ) and (ii) saturation readiness represented by ground water depth (GWD, d). Both parameters were reclassified firstly into four ordinal susceptibility classes (Low–Very High) and transformed

into standardized scores to a common scale of 1–4 to ensure consistency with the thresholds used (Table 1). The GSS class thresholds are according to Ilham et al. (2021) with the high/very-high boundary corresponding to the strain domain of Ishihara (1996), where liquefaction becomes significant at $\gamma \geq 10^{-2}$ and very large strain levels correspond to near-collapse conditions. The GWD class thresholds were modified from Hartantyo (2014), where the shallower the groundwater, the higher the susceptibility.

Table 1. Classification and Score of Parameters

No	Parameter	Class limits	Category	Score
1	GSS (x10^{-3})	$\gamma < 2.5$	Low	1
		$2.5 \leq \gamma < 10$	Moderate	2
		$10 \leq \gamma < 50$	High	3
		$\gamma > 50$	Very High	4
2	GWD (m)	$d > 5.3$	Low	1
		$3 < d \leq 5.3$	Moderate	2
		$2.05 < d \leq 3$	High	3
		$d \leq 2.05$	Very High	4

Then, the two scored layers were combined using a conjunctive geometric mean to represent the "two-condition" nature of liquefaction – high demand of deformation and high readiness of saturation – while avoiding the oversensitivity of a direct product. This integration strategy was selected because liquefaction occurrence is fundamentally controlled by the simultaneous presence of both mechanical susceptibility and groundwater availability. In contrast to additive approaches such as weighted overlay, where a high value of one variable can compensate for a low value of another, the conjunctive geometric mean behaves as a non-compensatory operator that progressively reduces the resulting susceptibility when either prerequisite condition is weak. This characteristic is considered more consistent with the physical requirements of liquefaction, where neither soil deformability nor groundwater saturation alone is sufficient to indicate elevated susceptibility.

The Liquefaction Susceptibility Index (LSI) was calculated as:

$$LSI = \sqrt{S_{GSS} \cdot S_{GWD}} \quad (4)$$

where $S_{GSS} \in \{1, 2, 3, 4\}$ and $S_{GWD} \in \{1, 2, 3, 4\}$. Equal weighting was used due to the unavailability of an independent geotechnical dataset (e.g. CPT, SPT, or liquefaction inventory data) to objectively calibrate the relative contribution of the two variables. The relative importance of mechanical versus hydrological controls may vary between geological settings, but to provide a transparent and reproducible framework, and to reduce subjectivity in the absence of calibration data, equal weights are assigned. More sophisticated approaches, such as AHP-based weighting, fuzzy logic integration, or probabilistic susceptibility modelling, may offer greater flexibility in representing expert knowledge and uncertainty; however, these methods require additional assumptions, calibration datasets, or validation information that were not available for the present screening-level assessment. This formulation limits the index to be between 1.00 and 4.00 and penalizes low values of either proxy to reduce compensability. Thus, higher LSI requires both deformability and shallow-groundwater conditions to be relatively high.

Final susceptibility levels were assigned using a mechanistic interaction matrix (Table 2) such that: (i) Very High susceptibility occurs only when both parameters are Very High; (ii) High susceptibility corresponds to combinations yielding LSI > 2.50 (e.g., Moderate–Very High, High–High, High–Very High, and Very High–Moderate); (iii) Moderate susceptibility reflects partial concurrence; and (iv) Low susceptibility corresponds to jointly weak controlling conditions.

Table 2. Rule-Based Interaction Matrix

GSS\GWD	1 (Low)	2 (Moderate)	3 (High)	4 (Very High)
1 (Low)	1.00 (Low)	1.41 (Low)	1.73 (Moderate)	2.00 (Moderate)
2 (Moderate)	1.41 (Low)	2.00 (Moderate)	2.45 (Moderate)	2.83 (High)
3 (High)	1.73 (Moderate)	2.45 (Moderate)	3.00 (High)	3.46 (High)
4 (Very High)	2.00 (Moderate)	2.83 (High)	3.46 (High)	4.00 (Very High)

Table 3. Final Classification of the integrated Liquefaction Susceptibility Index (LSI)

LSI Range	Susceptibility Level
1.00 – 1.50	Low
> 1.50 – 2.50	Moderate
> 2.50 – 3.50	High
> 3.50 - 4.00	Very High

To report and quantify spatially, the continuous LSI surface (1.00–4.00) was categorized into four non-overlapping numerical classes consistent with the interaction matrix (Table 3). These numerical intervals are directly related to the discrete geometric mean outcomes (1.00, 1.41, 1.73, 2.00, 2.45, 2.83, 3.00, 3.46, 4.00) and are interpretable in terms of the underlying evidence for the parameter. Within such a framework, LSI = 1.00 indicates minimum joint susceptibility (both parameters Low), LSI = 4.00 maximum joint susceptibility (maximization of the concurrence of the deformation demand and the saturation readiness), and Intermediate values quantify a progressively increasing joint susceptibility evidence.

4. Results and Discussion

4.1 GSS as an indicator of deformability

In order to (i) obtain insight into the spatial influence of deformability and saturation controls and (ii) highlight the limitations and potential biases of single-parameter zonation and advocate the necessity of a two-condition (conjunctive) approach, each proxy was evaluated separately for liquefaction susceptibility. In this work, "susceptibility" is understood as the relative, proxy-based propensity conditioned by deformability (GSS) and saturation (GWD), rather than a deterministic evaluation of triggering (e.g. a factor of safety in the CSR-CRR sense).

The first parameter is Ground Shear Strain (GSS). The GSS parameter is the maximum strain the ground surface can tolerate during an earthquake (Hanatha et al., 2023; Ina et al., 2020; Nakamura, 1997). GSS value from microtremor study is an important metric, because it is a ground deformation. High values of GSS often imply loose, unconsolidated, soft soil deposits which is a major requirement for liquefaction (Syamsuddin et al., 2024). Thus, in this work GSS is considered as proxy parameter for the deformability (mechanical susceptibility), where high strain potential does not mean liquefaction if the soil saturation conditions are not sufficient. The GSS classification thresholds adopted in this study were derived from previous investigations and provide a practical framework for regional-scale screening. Nevertheless, the applicability of these thresholds to Central West Lombok

remains subject to uncertainty because local geotechnical calibration data are not yet available. Small changes in threshold values may locally modify class assignments, particularly near class boundaries, although the broader regional pattern of higher deformability within the western alluvial corridor is expected to remain relatively stable.

The GSS surface was generated using ordinary kriging with the selected nugget-exponential variogram model. This model was selected after comparing nugget-linear, nugget-spherical, and nugget-exponential models using cross-validation statistics. The nugget-exponential model produced the best overall performance, with ME = -0.082 $\times 10^{-3}$, MAE = 6.181 $\times 10^{-3}$, and RMSE = 11.551 $\times 10^{-3}$. The selected nugget-exponential model was defined by a nugget of 20, exponential scale of 150, and length parameter of 3000 m. The resulting GSS grid ranged from 0.06 × 10^{-3} to 69.66 × 10^{-3} (Figure 3a), indicating that the model preserved the spatial variability required for susceptibility classification. However, the relatively high RMSE indicates that local extreme GSS values were not fully captured by the interpolation. Therefore, the GSS map should be interpreted as a regional deformation-demand trend rather than an exact site-specific prediction.

The map indicates that the high to extremely high GSS values (orange to red, 10.00 × 10^{-3} – 69.66 × 10^{-3}) are mostly distributed around the western shore (Labuapi, Gerung, Lembar) and a localized hotspot in the southern Gerung area. The lowest values (blue/green, 0.06 × 10^{-3} – 2.50 × 10^{-3}) are dominated in the Kuripan and the east half of Kediri sub-districts. This result is consistent with prior studies (Harsuko et al., 2020; Marjiyono, 2016) which identified the coast in the western portion of Lombok Island as a high susceptibility zone. The kriging standard deviation grid for the selected GSS model ranged from 5.922 $\times 10^{-3}$ to 11.754 $\times 10^{-3}$, with a mean value of 8.203 $\times 10^{-3}$ and a median value of 8.178 $\times 10^{-3}$. The coefficient of variation of the standard deviation grid was 0.088, indicating that the prediction uncertainty was spatially consistent across the study area. Nevertheless, the higher absolute uncertainty in GSS reflects stronger local variability in near-surface ground response.

The reclassification of the Ground Shear Strain (GSS) values resulted in the "Liquefaction Susceptibility Map based on GSS" (Figure 3(b)). The total size of the study area was 13852.02 Ha. Quantitatively, the 'Moderate' and 'Low' classifications dominated the map with a total coverage of 10183.33 Ha (73.51%) correspondingly. The 'Very High' class is confined to 111.36 Ha (0.80%) and 'High' class covers 3,557.33 Ha (25.68%). This pattern reveals that high deformability is spatially localized, mainly in the western coastal belt and a small hotspot in the Gerung region, and not uniformly distributed over the district. High GSS values are still spatially associated with the young unconsolidated Alluvial Formation (Qa). The nature of alluvial material, which comprises of loose elements including gravel, sand, clay, and peat (Mangga et al., 1994), is one of the drivers for the increase in seismic amplification and eventually the increase in liquefaction susceptibility (Refrizon et al., 2025).

However, moderate to low GSS classes dominate most of the study area, indicating lateral differences in surface layer stiffness and soil strain reactivity even across essentially identical surface units. This supports GSS as a better mechanical screening measure than a solitary indicator to determine the potential of liquefaction. This quantitative assessment validates the results of previous regional studies (Taruna et al., 2024) that highlight the importance of unconsolidated Quaternary deposits and additionally suggest that based on the microtremor analysis results, only certain segments of these deposits are highly prone to strain.

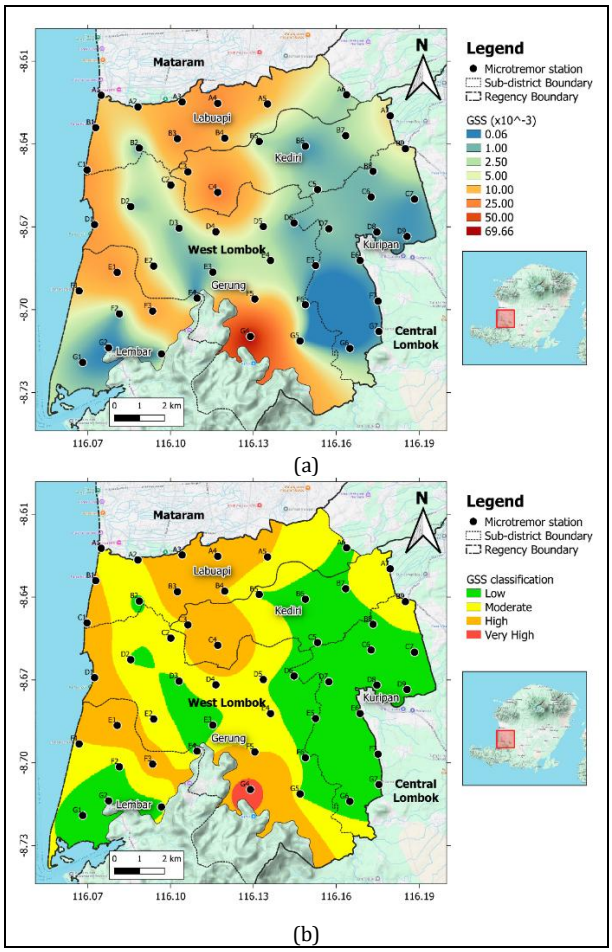

Fig. 3. (a) Spatial distribution of interpolated Ground Shear Strain (GSS; $\times 10^{-3}$) in the study area; (b) GSS-based susceptibility class (proxy for deformability) based on the score threshold in Table 1.

Meanwhile, the most dominant area in the study area is the area with the level of "Moderate" and "Low" liquefaction susceptibility, with a total area of 10,183.33 hectares (73.51%). The "Moderate" category of this area is 5,093.59 hectares (36.77%) and "Low" category of this area is 5,089.74 hectares (36.74%). The zones of lower susceptibility are associated with older, tougher and more consolidated geology. For example, the "Low" and "Moderate" zones in Kuripan District are geographically correlated with the distribution of Kalibabak Formation (TQb) and Kalipalung Formation (TQp) which consists of breccias and lava with more rigid properties. Similarly, the "Low" potential zone in Lembar District is connected with Pengulung Formation (Tomp) while the "Low" zone in Gerung District is associated with Kawangan Formation (Tomk). The increased consolidation and stiffness of these older geological units make the constituent materials of these units more resistant to liquefaction (Andrus & Bwambale, 2021). This result is consistent with the well-known fact that the underlying geological characteristics are the main governing elements for the soil response to the seismic loading (Civelekler et al., 2024; Hossain et al., 2025; Meng et al., 2022).

4.2 GWD as a saturation proxy

Depth to groundwater (GWD) was employed as proxy for saturation as liquefaction requires saturated (or near-saturated) granular materials (Dwiyantoro et al., 2023; Hu et al., 2021). The spatial pattern of GWD (Figure 4a) is consistent with topography-driven groundwater flow, where the configuration of the water table is commonly controlled by the relief of the land surface and boundary conditions (e.g., coastal base level), but modulated by hydrostratigraphic contrasts among geological units (Zhang et al., 2022).

The GWD surface was generated using ordinary kriging with the selected nugget-spherical variogram model. This model was selected after comparing nugget-linear, nugget-spherical, and nugget-exponential models. The nugget-spherical model produced the lowest MAE and RMSE, with ME = 0.014 m, MAE = 1.342 m, and RMSE = 1.996 m. The selected nugget-spherical model was defined by a nugget of 0.3, sill contribution of 3.5, and range of 2000 m. The resulting GWD grid ranged from 0.64 to 11.00 m, which preserved the groundwater-depth range required for susceptibility classification. Therefore, the nugget-spherical model was used as the final GWD interpolation model. The kriging standard deviation grid for the selected GWD model ranged from 0.772 to 2.010 m, with a mean value of 1.639 m and a median value of 1.672 m. The coefficient of variation of the standard deviation grid was 0.129, indicating moderate and relatively homogeneous prediction uncertainty. Higher uncertainty values should be interpreted as areas with lower interpolation confidence, especially where local groundwater variability is stronger or observation support is lower.

Sparse elevation contours indicate flat topography and the presence of Quaternary Alluvium (Qa). Accordingly, most of the groundwater occurs at shallow depths (green, 0.64 – 2.05 m) along the western shore of the study area. These low-relief alluvial plains are expected to have shallow unconfined aquifer conditions. Groundwater discharge to lowlands/coastal reaches tends to keep the water table near to the ground surface, hence promoting high saturation readiness. These low plains have high saturation and maximize liquefaction susceptibility (Mantap et al., 2025). Meanwhile in the Kediri another anomaly of deep groundwater (orange to red, 5.30 – 11.00 m) is found. This inland sector is a transition to higher ground, where even a slight change in elevation results in a thicker vadose-zone and changes the local hydraulic head relative to the land surface, leading to deeper measured GWD (Zhang et al., 2022). Moreover, the result of geological overlay suggests that some areas of Kediri area are bordering or composed of more consolidated volcanic units such as TQb and TQp Formations. In contrast to the Alluvium (Qa) unit, these units are characterized by a heterogeneous groundwater storage system regulated by cracks and rock strata. This diversity in hydrostratigraphic properties can produce a fall in the effective groundwater table and enhance the spatial heterogeneity of GWD values over relatively short distances (Melati et al., 2023).

The depth of groundwater table is dynamic and impacted by seasonal oscillations, therefore, the GWD map developed in this study is indicative of the time of measurement only. Therefore, the demarcation of the susceptibility zones is shifting during the wet season notably in the transition zones (Dwiyantoro et al., 2023). Therefore, GWD-based susceptibility classes should be treated as season-dependent indicators rather than hydrological conditions. Areas close to classification thresholds may move between susceptibility classes as groundwater levels move between wet and dry seasons. The overall pattern of shallow groundwater across the western coastal plain is likely to be retained but local susceptibility classifications may change over time.

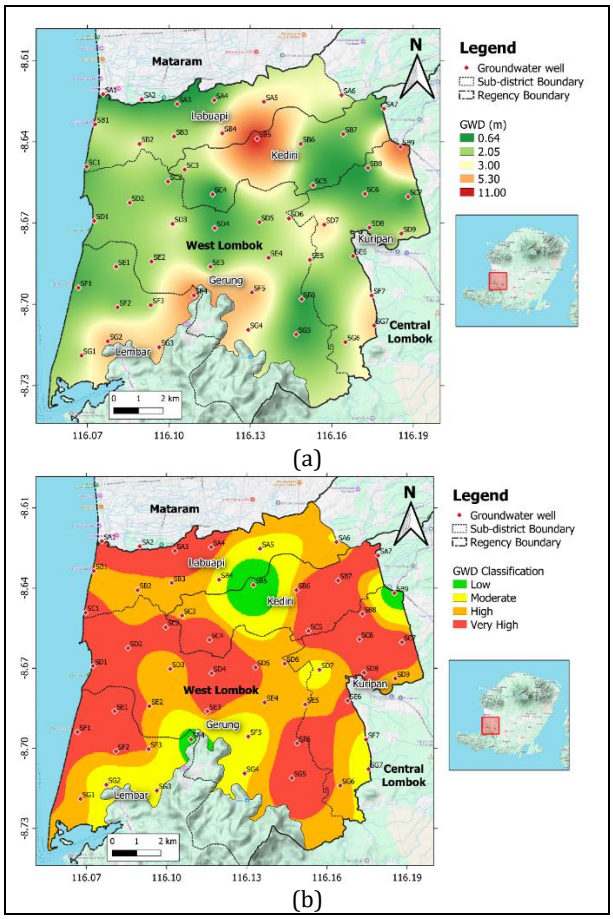

Fig. 4. (a) Spatial distribution of interpolated groundwater depth (GWD; m) in the study area. A smaller GWD value signifies a shallower groundwater level, and consequently a higher level of susceptibility. (b) GWD-based susceptibility classification as proxy for the degree of soil saturation, produced according to the score criteria in Table 1. The smaller the value of GWD, the higher the level of preparedness of soil saturation.

The "Liquefaction Susceptibility Map based on GWD" (Figure 4(b)) was developed from the inverse relationship (Table 1) where shallow GWD values (<2.05 m) were classified as "Very High" potential category based on the empirical relationship between groundwater level and liquefaction occurrence reported by Hartantyo et al. (2014). In quantitative words, the GWD based model suggests that 77.24% of the overall study area (10,699.63 Ha) is within the "High" to "Very High" categories. This shows that the hydrological conditions conducive for liquefaction are common in the studied area. Specifically, "Very High" category occupies an area of 5,846.06 Ha (42.20%) whereas "High" category occupies an area of 4,853.57 Ha (35.04%). The dominance of the high susceptibility category is in agreement with the general understanding that shallow groundwater levels or rising groundwater levels can greatly enhance the liquefaction risk by increasing the thickness of the saturated soil layer, which may lead to the generation of excess pore pressure under cyclic loading (Li et al., 2025).

More notably, the GWD map displays a large contrast when compared to the GSS map. While the GSS map is dominated by "Moderate" to "Low" categories, the GWD

map exhibits "High" to "Very High" categories, meaning many places satisfy hydrological conditions for liquefaction but not mechanical ones. This means that many of the places satisfy the hydrological conditions for liquefaction but not the mechanical deformability conditions. Therefore, relying solely on GWD parameters may lead to false positives, a limitation consistent with recent studies emphasizing that groundwater data must be assessed alongside soil conditions and seismic shaking to prevent misclassification (Galupino & Dungca, 2023). The GSS classification in the Kediri District is largely "Low", with only a few local zones in the "Moderate" category. The GWD map reveals zones of reduced susceptibility due to deeper groundwater levels, thereby minimizing the possibility of soil saturation. In contrast, in Kuripan District, the GSS map reveals modest mechanical susceptibility, however the GWD map is dominated by "High" to "Very High" categories, showing that soil saturation conditions can be fulfilled even with moderately stiff soil conditions. This mismatch between the mechanical (GSS) and hydrological (GWD) criteria highlights the fragility of a zoning system based on a single parameter and the need for an integrated, conjunctive susceptibility model (Dwiyantoro et al., 2023).

4.3 GSS-GWD fusion: Combined susceptibility

This integrated assessment integrates two complementary important liquefaction prerequisites, the soil deformability (GSS) and the soil saturation readiness (GWD), into a single analytic surface (screening surface). This approach is compatible with regional scale research examining liquefaction susceptibility as a result of the interaction of numerous regulating elements, rather than based on a single parameter (Zumpano et al., 2022). These two parameters are combined using the conjunctive geometric mean approach without considering the weight of the reclassified class scores (Table 1) to obtain a continuous Liquefaction Susceptibility Index (LSI) map as shown in Figure 5(a). The integrated susceptibility model should be interpreted as a proxy-based screening framework rather than direct evidence of liquefaction occurrence. The resulting LSI values express the spatial concurrence of two prerequisite conditions for liquefaction (deformability and saturation) but do not quantify liquefaction triggering probability or factor of safety.

The LSI values obtained ranged from 1.00 (least susceptible level) to 3.46 (most susceptible level recorded). The high LSI values are centered throughout the western coastal plain and a few sites in the western sector of the research region. The inland locations often exhibit lower integrated susceptibility levels. This trend is consistent with the features of coastal areas and low alluvial plains that are anticipated to be more vulnerable to liquefaction because of the potential occurrence of higher shallower groundwater tables (Manoharan & Ganapathy, 2023).

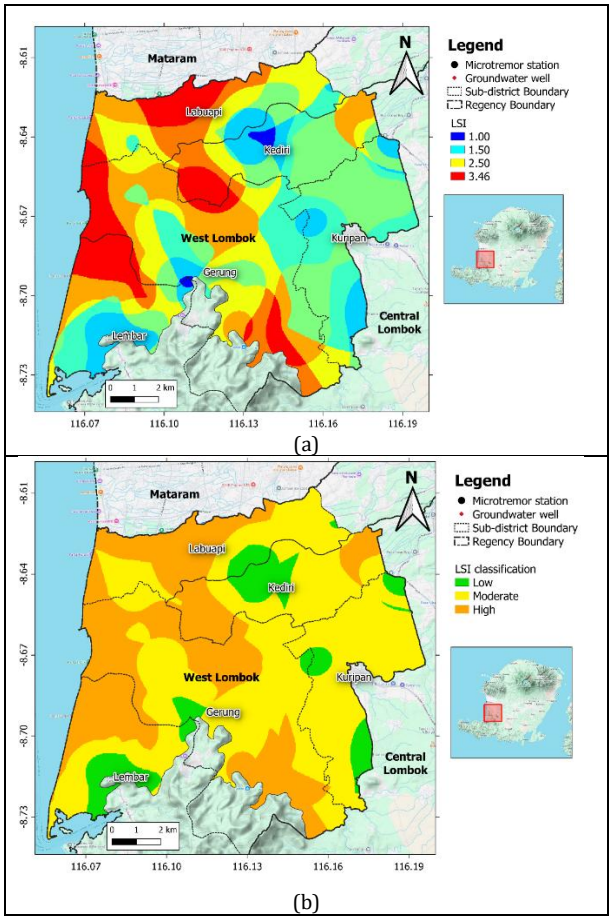

Fig. 5. (a) Map of LSI values acquired from the integration of the conjunctive geometric mean on the GSS and GWD layers; (b) Liquefaction susceptibility class zoning produced from the LSI model on the conjunctive geometric mean.

Table 4. Liquefaction Potential Category Area Coverage Based on GSS, GWD and Integrated Models

Model	Area (Ha)				
	Very High	High	Moderate	Low	Total
GSS	111.36 (0.80 %)	3,557.33 (25.68 %)	5,093.59 (36.77 %)	5,089.74 (36.74 %)	13,852.02 (100 %)
GWD	5,846.06 (42.20 %)	4,853.57 (35.04 %)	2,614.97 (18.88 %)	537.41 (3.88 %)	13,852.02 (100 %)
Integrated (GSS & GWD)	0.00 (0.00 %)	4,819.70 (34.79 %)	7,674.71 (55.40 %)	1,357.62 (9.80 %)	13,852.02 (100 %)

Theoretically, the maximum value of the geometric mean is 4.00, which occurs only when both of the input variables are at their highest class at the same moment, i.e. 'Very High' in GSS and 'Very High' in GWD in the same grid cell. However, the mapping results reveal a maximum observed value of 3.46 which implies that the strongest co-occurrence is a 'High'–'Very High' combination, not a 'Very High'–'Very High' combination. This conclusion is in line with the class distribution of the input layers where the 'relatively High' class in GSS is relatively limited (111.36 Ha; 0.80%) and the 'Very High' class in GWD is extensively dispersed in the study region (5846.06 Ha; 42.20%). This geographical mismatch shows that the zones of maximal soil deformability do not correlate to the zones of shallowest ground water at the grid-cell scale. This mismatch hinders the accomplishment of the theoretical maximum LSI of 4.00, thus explaining the absence of the integrated 'Very High' class (0.00 Ha). The interaction matrix further demonstrates that the 'High' class can also be obtained by asymmetric combinations of 'Moderate-Very High' or 'Very High-Moderate' and not only the 'High-High' criteria.

For interpretation, the criteria in Table 3 were utilized to reclassify the continuous LSI surface to generate the Integrated Liquefaction Susceptibility Map (Figure 5(b)). The resulting classes are summarized in Table 4 as 0.00 Ha (0.00%) 'Very High', 4819.70 Ha (34.79%) 'High', 7674.71 Ha (55.40%) 'Moderate' and 1357.62 Ha (9.80%) 'Low'. In the joint-evidence framework, the "High" class reflects places where neither controlling factor is low and at least one proxy supports high to very high conditions. Inconsistent combinations are down-graded spatially, decreasing the overestimation of single-parameter techniques.

Uncertainty in the integrated susceptibility map originates from several sources, including interpolation of point observations, parameter classification thresholds, and the conjunctive integration procedure itself. Because GSS and GWD were first transformed into interpolated continuous surfaces and subsequently reclassified into ordinal scores, uncertainty associated with each processing step may propagate into the final LSI values. Therefore, susceptibility boundaries should be interpreted as transitional zones rather than precise spatial limits. The kriging standard deviation results indicate that interpolation uncertainty is mainly relevant near class boundaries and in areas with lower local observation support. This issue is more important for GSS because its cross-validation RMSE was higher than that of GWD, reflecting stronger local variability and the influence of extreme values.

The influence of observation density was also considered in interpreting the integrated susceptibility map. The 52 observation points had a mean nearest-neighbor spacing of 1394.8 m and a median spacing of 1419.7 m, with local spacing ranging from 864.5 to 1756.2 m. During cross-validation, each kriging estimate used an average of 36.38 data points, with a minimum of 18 and a maximum of 51 points. These values indicate that the interpolation was supported by moderate regional observation density. Therefore, the GWD, GSS, and LSI maps should be interpreted as regional-scale susceptibility screening products rather than site-specific predictions. Areas farther from observation points and areas close to class thresholds should be interpreted with greater caution.

The integrated approach greatly decreases the over-flagging induced by saturation with the 'High' class confined to 34.79% (4819.70 Ha) where the shallow groundwater is supported by soil with enough deformability compared to the GWD-only model (77.24% High-Very High). In contrast, the combined 'High' extent is bigger than the GSS-only model (High–Very High = 26.48%), demonstrating that mechanically mild zones may nevertheless have enhanced susceptibility when associated with chronically shallow groundwater conditions. In summary, the integrated map strengthens the spatial pattern by centering 'High' susceptibility throughout the western sector including the coastal belt, while awarding the rest of the regency to the 'Moderate' class (55.40%), resulting in a sharper differentiation than single-layer zonations.

At the sub-district level, the 'High' susceptibility is mostly associated to the coastal and alluvial plain settings. In the western–northwestern sector, Labuapi shows clustering of High zones, with Gerung localizing High patches within wider Moderate zones. The western sector of Lembar has a strong coastal-belt signal with minor small Low pockets to the southwest. The inland areas generally have lesser susceptibility: Kediri is dominated by the Moderate class with a notable Low anomaly matching to deeper groundwater conditions, whereas Kuripan is predominantly Moderate to Low, consistent with modest contribution from GSS. Together, the patterns suggest that susceptibility is essentially regulated by the spatial overlap of deformability and saturation, giving a better foundation for directing future investigations. These spatial trends are further contextualized by contrasting the integrated susceptibility corridor with regional screening references and independent subsurface evidence.

Although qualitative comparison with regional susceptibility maps and independent geophysical observations provides indirect support for the identified spatial patterns, the present model has not been validated using CPT measurements, SPT data, borehole observations, or documented liquefaction inventories. Consequently, the identified susceptibility zones should not be interpreted as confirmed liquefaction occurrences but rather as areas where conditions may be more favorable for liquefaction development under strong seismic loading. Therefore, validation in the present study is limited to qualitative comparison with independent regional datasets.

The national liquefaction susceptibility atlas of the Geological Agency reveals non-negligible susceptibility over the western Lombok lowland and alluvial corridor (including the Mataram–West Lombok plain), corroborating the existence of elevated susceptibility zones at the regional scale (Buana et al., 2020). In addition, geophysical evidence from the adjacent areas in western Lombok showed sand-dominated subsurface layers with depths greater than ~30 m and local shallow groundwater conditions (<2 m) based on electrical resistivity tomography surveys (Sudrajat et al., 2026), both of which are favorable conditions for liquefaction under strong seismic loading. These independent datasets offer indirect but consistent support for the identified coastal-plain susceptibility corridor. Nevertheless, future validation should incorporate georeferenced liquefaction inventories and targeted geotechnical investigations (e.g., CPT, SPT, boreholes, and trenching) to evaluate the predictive performance of the screening-level model.

Nonetheless, the map given here still represents a screening product based on proxies. Groundwater depth was recorded in one campaign during dry season (August 2025) which implies the saturation component is a temporal snapshot which might not be typical of seasonal variations. This constraint is especially noteworthy since groundwater fluctuations can considerably modify liquefaction susceptibility over time (Li et al., 2025; Zumpano et al., 2022). Additionally, the lack of site-specific geotechnical parameters and a georeferenced liquefaction inventory prohibits event-based validation. Recent studies show that CPT- and SPT-derived parameters are important for robust liquefaction evaluation beyond screening-level assessments (Ahamad et al., 2025). The identified 'High' susceptibility zones should therefore be regarded as priority targets for future geotechnical investigation rather than deterministic predictions of liquefaction occurrence. Verification through CPT, SPT, borehole investigations, groundwater monitoring, and future liquefaction inventories will be necessary to evaluate and refine the screening-level susceptibility patterns presented in this study.

5. Conclusion

The present study developed a screening-level liquefaction susceptibility assessment for Central West Lombok by integrating the ground deformability (GSS) and

groundwater depth (GWD) through an unweighted conjunctive geometric mean to derive the Liquefaction Susceptibility Index (LSI). The single-parameter maps show opposite trends. The GSS-based map is mainly Moderate-Low, implying that higher deformability is spatially localized, while the GWD-based map classifies a large portion of the region as High-Very High, indicating that groundwater conditions alone may over-flag susceptibility if considered separately. The integrated LSI offers a more defensible screening zonation by constraining susceptibility by conjunctive-biased fusion to generate 34.79% High (4819.70 Ha), 55.40% Moderate (7674.71 Ha), and 9.80% Low (1357.62 Ha), and no Very High class (0.00 Ha) with a maximum observed LSI of 3.464 – i.e., no mapped areas show the simultaneous occurrence of very-high deformability and very-shallow groundwater conditions. These results should be interpreted as indicators of relative susceptibility patterns rather than direct predictions of liquefaction occurrence.

Spatially, areas with elevated susceptibility are concentrated in the western coastal belt and adjacent lowlands, where favorable mechanical and hydrological conditions tend to coexist. Accordingly, the resulting map is intended as a regional-scale screening and prioritization tool for future geotechnical investigations, including CPT/SPT testing, borehole logging, trenching, and detailed site characterization, rather than as a deterministic assessment of liquefaction hazard. Several sources of uncertainty should be considered when interpreting the results. These include uncertainty associated with kriging interpolation of GSS and GWD observations, seasonal groundwater fluctuations that may modify groundwater depth classes, sensitivity of susceptibility classifications to selected threshold values, and the absence of direct validation using CPT data, SPT measurements, borehole information, or documented liquefaction inventories. Consequently, susceptibility boundaries should be regarded as approximate transition zones rather than precise spatial limits. Future studies should include re-measurement of groundwater levels during rainy and dry seasons, more detailed quantification of interpolation uncertainty, and compilation of a georeferenced liquefaction event inventory through field mapping, historical reports and remote sensing data. Integration with geotechnical datasets and systematic validation efforts will be necessary to evaluate, refine, and potentially transform the present screening-level susceptibility framework into a more robust engineering-based assessment.

Acknowledgment

The authors gratefully acknowledge the financial support from the Research and Community Service Institute (LP2M) of UIN Mataram through the 2025 Output-Based Standard Cost Research Assistance Program..

References

Aditama, M. R., Sunan, H. L., Tri Laksono, F. A., Ramadhan, G., Iswahyudi, S., & Fadlin. (2021). Integrated Subsurface Analysis of Thickness and Density for Liquefaction Hazard: Case Study of South Cilacap Region, Indonesia. Journal of Geoscience, Engineering, Environment, and Technology, 6(1), 58–66. https://doi.org/10.25299/jgeet.2021.6.1.5892

Alonso-Pandavenes, O., Torrijo, F. J., & Torres, G. (2024). Analysis of the Liquefaction Potential at the Base of the San Marcos Dam (Cayambe, Ecuador)—A Validation in the Use of the Horizontal-to-Vertical Spectral Ratio. Geosciences, 14(11), 306. https://doi.org/10.3390/geosciences14110306

Andrus, R. D., & Bwambale, B. (2021). Assessing the Effect of Aging on Soil Liquefaction Resistance (pp. 163–173). https://doi.org/10.1007/978-981-16-1468-2_8

Bao, X., Jin, Z., Cui, H., Chen, X., & Xie, X. (2019). Soil liquefaction mitigation in geotechnical engineering: An overview of recently developed methods. Soil Dynamics and Earthquake Engineering, 120, 273–291. https://doi.org/10.1016/j.soildyn.2019.01.020

Buana, T. W., Hermawan, W., Rahdiana, R. N., Widyaningrum, R., Wahyudin, Hasibuan, G., Wiyono, & Sollu, W. P. (2020). Atlas Zona Kerentanan Likuefaksi Indonesia (2nd ed.). Badan Geologi Kementerian Energi dan Sumber Daya Mineral.

Chung, J.-W., & Rogers, J. D. (2013). Influence of Assumed Groundwater Depth on Mapping Liquefaction Potential. Environmental & Engineering Geoscience, 19(4), 377–389. https://doi.org/10.2113/gseegeosci.19.4.377

Civelekler, E., Afacan, K. B., & Okur, D. V. (2024). Effect of site specific soil characteristics on the nonlinear ground response analysis and comparison of the results with equivalent linear analysis. Journal of Applied Geophysics, 220, 105250. https://doi.org/10.1016/j.jappgeo.2023.105250

Cox, B. R., Cheng, T., Vantassel, J. P., & Manuel, L. (2020). A statistical representation and frequency-domain window-rejection algorithm for single-station HVSR measurements. Geophysical Journal International, 221(3), 2170–2183.

Dwiyantoro, W., Fathani, T. F., & Adi, A. D. (2023). Influence of Groundwater Table Fluctuation on Liquefaction Potential Analysis Using Cyclic Stress Approach. IOP Conference Series: Earth and Environmental Science, 1184(1), 012006. https://doi.org/10.1088/1755-1315/1184/1/012006

Fukushima, Y., Köse, O., Yürür, T., Volant, P., Cushing, E., & Guillande, R. (2002). Attenuation Characteristics of Peak Ground Acceleration from Fault Trace of The 1999 Kocaeli (Turkey) Earthquake and Comparison of Spectral Acceleration with Seismic Design Code. Journal of Seismology, 6, 379–396.

Galupino, J., & Dungca, J. (2023). Estimating Liquefaction Susceptibility Using Machine Learning Algorithms with a Case of Metro Manila, Philippines. Applied Sciences, 13(11), 6549. https://doi.org/10.3390/app13116549

Hanatha, F. D., Indriatmoko, T. W., & Qurrotu'aeni, W. S. (2023). Analysis of Soil and Rock Strength Using Vs30 Value and Ground Shear Strain Based on Microtremor Data in the Pindul Cave Area, Gunung Kidul, Yogyakarta. Jurnal Geosaintek, 9(1), 29. https://doi.org/10.12962/j25023659.v9i1.16257

Harsuko, M. R. C., Z., Z., Nugraha, A. D., Muzli, M., Sahara, D. P., Puspito, N. T., Husni, Y. M., Prabowo, B. S., & Sarjan, A. F. N. (2020). Analysis of H/V Ratio Curve to Estimate Seismic Hazard Vulnerability in Lombok Island, West Nusa Tenggara, Indonesia. Jurnal Geofisika, 18(1), 1. https://doi.org/10.36435/jgf.v18i1.432

Hartantyo, E., Brotopuspito, K. S., Sismanto, & Waluyo. (2014). Correlation of Shallow Groundwater Levels with The Liquefaction Occurrence Cause By May 2006 Earthquake In The South Volcanic-clastic Sediments Yogyakarta , Indonesia. International

Journal of Applied Sciences, 5(1), 1–8.
Hatmoko, J. T., & Suryadharma, H. (2015). Prediction of liquefaction potential study at Bantul Regency the province of special region of Yogyakarta Indonesia. Procedia Engineering, 125, 311–316. https://doi.org/10.1016/j.proeng.2015.11.068
Hossain, A. S. M. F., Saeidi, A., Salsabili, M., Nastev, M., Suescun, J. R., & Bayati, Z. (2025). A Review of Parameters and Methods for Seismic Site Response. Geosciences, 15(4), 128. https://doi.org/10.3390/geosciences15040128
Hu, J., Tan, Y., & Zou, W. (2021). Key factors influencing earthquake-induced liquefaction and their direct and mediation effects. PLOS ONE, 16(2), e0246387. https://doi.org/10.1371/journal.pone.0246387
Hutchings, S. J., & Mooney, W. D. (2021). The Seismicity of Indonesia and Tectonic Implications. Geochemistry, Geophysics, Geosystems, 22(9), 1–42. https://doi.org/10.1029/2021GC009812
Ilham, I., & Sani, M. A. (2025). Microtremor based seismic vulnerability assessment of UIN mataram campus II, Lombok. Compton: Jurnal Ilmiah Pendidikan Fisika, 12(1), 106–120. https://doi.org/10.30738/cjipf.v12i1.19620
Ilham, Prabowo, U. N., & Sismanto. (2021). Mapping the Potential Liquefaction Area in Yogyakarta City Based on Ground Shear Strain Data. Jurnal Fisika Dan Aplikasinya, 17(3), 74–78.
Ina, S., Yuliyanto, G., & Irham, M. N. (2020). Calculating ground shear strain (GSS) of microtremor data using graphical user interface python programming. Journal of Physics: Conference Series, 1524(1), 012015. https://doi.org/10.1088/1742-6596/1524/1/012015
Irsyam, M., Widiyantoro, S., Natawidjaja, D. H., Meilano, I., Rudyanto, A., Hidayati, S., Triyoso, W., Hanifa, N. R., Djarwadi, D., Faizal, L., & Sunarjito. (2017). Peta Sumber dan Bahaya Gempa Indonesia Tahun 2017. Badan Penelitian dan Pengembangan Kementerian Dalam Negeri Republik Indonesia.
Ishihara, K. (1996). Soil Behaviour in Earthquake Geotechnics. Clarendon Press.
Jalil, A., Fathani, T. F., Satyarno, I., & Wilopo, W. (2021). Liquefaction in Palu: the cause of massive mudflows. Geoenvironmental Disasters, 8(1), 21. https://doi.org/10.1186/s40677-021-00194-y
Konno, K., & Ohmachi, T. (1998). Ground-motion characteristics estimated from spectral ratio between horizontal and vertical components of microtremor. Bulletin of the Seismological Society of America, 88(1), 228–241. https://doi.org/10.1785/bssa0880010228
Kurniawan, C. W., Yatini, Y., & Pramono, S. (2023). Application of Ground Shear Strain (GSS) for Mapping Liquefaction Potential in Palu, Central Sulawesi, Indonesia. International Journal of Scientific and Research Publications, 13(2), 64–71. https://doi.org/10.29322/IJSRP.13.02.2023.p13407
Kusuma, W. H., & Sanny, T. A. (2022). Analysis of Ground Shear Strain (GSS) In Mapping, Liquefaction Vulnerability Potential Using HVSR (Horizontal To Vertical Spectral Ratio) Method. Case Study: Sepaku Subdistrict, North Penajam Paser Regency, East Kalimantan. IOP Conference Series: Earth and Environmental Science, 1031(1), 012027. https://doi.org/10.1088/1755-1315/1031/1/012027
Li, Y., Wang, R., Ma, H., & Zhang, J.-M. (2025). Rising groundwater table due to restoration projects amplifies earthquake induced liquefaction risk in Beijing. Nature Communications, 16(1), 1466. https://doi.org/10.1038/s41467-025-56525-2
Loviknes, K., Cotton, F., & Weatherill, G. (2024). Exploring inferred geomorphological sediment thickness as a new site proxy to predict ground-shaking amplification at regional scale: application to Europe and eastern Türkiye. Natural Hazards and Earth System Sciences, 24(4), 1223–1247. https://doi.org/10.5194/nhess-24-1223-2024
Malawani, M. N., Hadmoko, D. S., Lavigne, F., Agniy, R. F., Hayat, D. M., Astabella, R. D., Laksono, A., Syamsuddin, S., & Mutaqin, B. W. (2024). Review on the Impacts of the Samalas Eruption (1257 CE) to the Hydrogeological Conditions of Mataram, Lombok, Indonesia. Indonesian Journal on Geoscience, 11(3), 339–348. https://doi.org/10.17014/ijog.11.3.339-348
Manan, A., Puspitafuri, C., Chahyani, R., Irawati, & Pertiwi, I. I. (2023). Identification Of Shear Strain On The Surface Ground Of Wangi-Wangi Island, Southeast Sulawesi, Indonesia, Using Nakamura's Technique and The Possibility Of Its Impacts. Journal of Geoscience, Engineering, Environment, and Technology, 8(4), 275–280. https://doi.org/10.25299/jgeet.2023.8.4.11780
Mangga, S. A., Atmawinata, S., Hermanto, B., Setyogroho, B., & Amin, T. C. (1994). Peta Geologi Lembar Lombok, Nusa Tenggara Barat.
Manoharan, S. G., & Ganapathy, G. P. (2023). GIS based urban social vulnerability assessment for liquefaction susceptible areas: a case study for greater Chennai, India. Geoenvironmental Disasters, 10(1), 1. https://doi.org/10.1186/s40677-022-00230-5
Mantap, B., P., M. W., & Parwito. (2025). Analysis of Soil Stability and Foundation Bearing Capacity in Infrastructure Development in Earthquake-Prone Areas. Journal of Engineering and Applied Technology, 1(2), 22–29. https://doi.org/https://doi.org/10.65310/rsxqfa42
Marjiyono, M. (2016). Potensi Penguatan Gelombang Gempabumi oleh Sedimen Permukaan Kota Mataram, Nusa Tenggara Barat. Jurnal Lingkungan Dan Bencana Geologi, 7(3), 135–144.
Melati, M. D., Athayde, G. B., Fan, F. M., Garcia, L. H., & de Vasconcelos Muller Athayde, C. (2023). Monitoring groundwater storage in a fractured volcanic aquifer system. Environmental Monitoring and Assessment, 195(3), 385. https://doi.org/10.1007/s10661-023-10978-4
Meng, S. bo, Zhao, J. wei, Liu, Z. xian, & Jin, W. (2022). Prediction and Modeling for Local Site Amplification Effect of Ground Motion: Exploring Optimized Machine Learning Approaches. Pure and Applied Geophysics, 8(2), 1592–1621.
Mulyana, G. D., Antosia, R. M., & Nathania, E. Y. (2026). Soft Layer Identification in Kedamaian District Using the HVSR-Derived Shear Wave Velocity Distribution. Journal of Geoscience, Engineering, Environment, and Technology, 11(1), 129–139. https://doi.org/10.25299/jgeet.2026.11.1.25294
Mustafa, R., Prasad Singh, A., & Ghani, S. (2025). Liquefaction assessment of soil based on SPT and CPT data using novel machine learning techniques: a

practical solution. Modeling Earth Systems and Environment, 11(3), 218. https://doi.org/10.1007/s40808-025-02404-0

Nakamura, Y. (1997). Seismic Vulnerability Indices For Ground and Structures Using Microtremor. World Congress on Railway Research, 1, 1–7.

Nakamura, Y. (2008). On the H/V Spectrum. The 14th World Conference on Earthquake Engineering, 1–10. http://117.120.50.114/papers/14wcee/14wcee_hv.pdf

Nakamura, Y. (2019). What is the Nakamura method? Seismological Research Letters, 90(4), 1437–1443. https://doi.org/10.1785/0220180376

Pebrianto, F., & Hidayat, A. A. N. (2018). Ini Data Lengkap Kerusakan Gempa Lombok Versi BNPB. https://nasional.tempo.co/read/1515374/antisipasi-korban-bmkg-berbagi-mitigasi-bencana-di-kawasan-selatan-jawa

Pemerintah NTB. (2024). Peraturan Daerah (Perda) Provinsi Nusa Tenggara Barat Nomor 5 Tahun 2024 tentang Rencana Tata Ruang Wilayah Provinsi Nusa Tenggara Barat Tahun 2024-2044. Jaringan Dokumentasi Dan Informasi Produk Hukum. https://jdih.ntbprov.go.id/produk-hukum/perda-nomor-5-tahun-2024

Prabowo, U. N., Ferdiyan, A., & Amalia, A. F. (2021). The Soft Layer Thickness Estimation using Microtremor Measurement to Identify Landside Potential in Watukumpul, Central Java, Indonesia. Journal of Geoscience, Engineering, Environment, and Technology, 6(1), 16–23. https://doi.org/10.25299/jgeet.2021.6.1.5436

Rachmat, H., Rosana, M. F., Wirakusumah, A. D., & Jabbar, G. A. (2016). Petrogenesis of Rinjani Post-1257-Caldera-Forming-Eruption Lava Flows. Indonesian Journal on Geoscience, 3(2), 107–126. https://doi.org/10.17014/ijog.3.2.107-126

Refrizon, Fadli, D. I., Sumanjaya, E., Maulidiyah, A., Hardianza, M., & Hardiansyah, D. (2025). Seismic microzonation in Bengkulu City, Indonesia: insights for resilient planning after 2000 Mw 7.9 and 2007 Mw 8.4 earthquakes. Bulletin of Earthquake Engineering, 23(8), 3085–3107. https://doi.org/10.1007/s10518-025-02168-z

Saputri, D., & Pujiastuti, D. (2020). Analisis Kecocokan Nilai Percepatan Tanah Pulau Lombok Berdasarkan Perhitungan Empiris dengan Data Percepatan Tanah dari Akselerograf di Stasiun Mataram. Jurnal Fisika Unand, 9(1), 79–84. https://doi.org/10.25077/jfu.9.1.79-84.2020

Sarah, D., & Soebowo, E. (2013). Liquefaction Due to the 2006 Yogyakarta Earthquake : Field Occurrence and Geotechnical Analysis. Procedia Earth and Planetary Science, 6, 383–389. https://doi.org/10.1016/j.proeps.2013.01.050

Sasmi, A. T., Nugraha, A. D., Muzli, M., Widiyantoro, S., Zulfakriza, Z., Wei, S., Sahara, D. P., Riyanto, A., Puspito, N. T., Priyono, A., Greenfield, T., Afif, H., Supendi, P., Daryono, D., Ardianto, A., Syahbana, D. K., Husni, Y. M., Prabowo, B. S., & Narotama Sarjan, A. F. (2020). Hypocenter and Magnitude Analysis of Aftershocks of the 2018 Lombok, Indonesia, Earthquakes Using Local Seismographic Networks. Seismological Research Letters, 91(4), 2152–2162. https://doi.org/10.1785/0220190348

Simandjuntak, T. O. (2014). Tektonika (S. Tjokrosapoetro, Ed.). Pusat Survei Geologi Bandung.

Soebowo, E., Tohari, A., & Sarah, D. (2007). Studi Potensi Likuifaksi di Daerah Zona Patahan Opak Patalan - Bantul, Jogjakarta. Proseding Seminar Geoteknologi Kontribusi Ilmu Kebumian Dalam Pembangunan Berkelanjutan.

Sudrajat, Y., Arisbaya, I., Handayani, L., Gaol, K. L., Mukti, M. M., Sugiarto, B., Syamsuddin, Mutaqin, B. W., Virmoux, C., & Lavigne, F. (2026). Electrical resistivity tomography for geohazard assessment in West Lombok's alluvial plain. Geosystems and Geoenvironment, 5(2), 100487. https://doi.org/10.1016/j.geogeo.2025.100487

Supartoyo, Hidayati, S., & Omang, A. (2018). Dampak Permukaan Gempa Lombok Tanggal 5 Agustus 2018. In M. Irsyam, N. R. Hanifa, & D. Djarwadi (Eds.), Kajian Rangkaian Gempa Lombok Provinsi Nusa Tenggara Barat (Pertama, 8). Pusat Penelitian dan Pengembangan Perumahan dan Pemukiman, Badan Penelitian dan Pengembangan, Kementerian Pekerjaan Umum dan Perumahan Rakyat.

Supartoyo, Robiana, R., Natalia, M. C., & Hespiantoro, S. (2020). Dampak Gempa Lombok Tahun 2018. Geominerba, 5(1), 61–76.

Syafaat, M. B., Buana, L. A. T. A., Putra, D. P. E., & Kuncoro, D. A. (2024). Hydrogeology Conceptual Model of Meninting Dam and Its Surrounding Area, West Lombok Regency, West Nusa Tenggara, Indonesia. IOP Conference Series: Earth and Environmental Science, 1291(1), 1–8. https://doi.org/10.1088/1755-1315/1291/1/012020

Syamsuddin, E., Maulana, A., Hamzah, A., & Irfan, U. R. (2024). Assessing soil vulnerability in Petobo post-liquefaction zone, Palu, Central Sulawesi: A microzonation study utilizing microtremor measurements. Journal of Degraded and Mining Lands Management, 11(3), 5805–5816. https://doi.org/10.15243/jdmlm.2024.113.5805

Taruna, R. M., Septiadhi, A., Sungkono, Mase, L. Z., & Mashuri. (2024). Preliminary Assessment of Liquefaction Vulnerability using Microtremor Analysis in North Lombok. Journal of Physics: Conference Series, 2866(1), 1–6. https://doi.org/10.1088/1742-6596/2866/1/012061

Towhata, I. (2008). Geotechnical Earthquake Engineering (W. Wu & R. I. Borja, Eds.). Springer.

Upomo, T. C., Chang, M., Kusumawardani, R., Prayitno, G. A., Huang, R.-C., & Fansuri, M. H. (2024). Preliminary Field Study of the Petobo Flow Slide After the 2018 Indonesia Palu Liquefaction. In Earth and Environmental Science Earth and Environmental Science (R0) (pp. 19–22). https://doi.org/10.1007/978-3-031-43218-7_5

USGS. (2018). M 6.9 - 36 km NW of Labuan Lombok, Indonesia. Earthquake Hazards Program. https://earthquake.usgs.gov/earthquakes/eventpage/us1000g3ub/executive

van Ginkel, J., Ruigrok, E., Wentinck, R., & Herber, R. (2022). Amplification Behaviour of Compressional Waves in Unconsolidated Sediments. Frontiers in Earth Science, 10, 1–17. https://doi.org/10.3389/feart.2022.812658

Wathelet, M., Chatelain, J. L., Cornou, C., Giulio, G. Di, Guillier, B., Ohrnberger, M., & Savvaidis, A. (2020). Geopsy: A user-friendly open-source tool set for ambient vibration processing. Seismological Research Letters,

91(3), 1878–1889. https://doi.org/10.1785/0220190360

Yatini, Putra, A. K., & Paripurno, E. T. (2023). An Application of HVSR Method on Microtremor Data for Analysis of Earthquake Potential in Candipuro District, Lumajang, Indonesia. Journal of Geoscience, Engineering, Environment, and Technology, 8(4), 288–294.

Youd, T. L., Idriss, I. M., Andrus, R. D., Arango, I., Castro, G., Christian, J. T., Dobry, R., Finn, W. D. L., Harder, L. F., Hynes, M. E., Ishihara, K., Koester, J. P., Liao, S. S. C., Marcuson, W. F., Martin, G. R., Mitchell, J. K., Moriwaki, Y., Power, M. S., Robertson, P. K., … Stokoe, K. H. (2001). Liquefaction Resistance of Soils: Summary Report from the 1996 NCEER and 1998 NCEER/NSF Workshops on Evaluation of Liquefaction Resistance of Soils. Journal of Geotechnical and Geoenvironmental Engineering, 127(10), 817–833. https://doi.org/10.1061/(ASCE)1090-0241(2001)127:10(817)

Zhang, X., Jiao, J. J., & Guo, W. (2022). How Does Topography Control Topography-Driven Groundwater Flow? Geophysical Research Letters, 49(20). https://doi.org/10.1029/2022GL101005

Zumpano, V., Pisano, L., Filice, F., Ugenti, A., de Lucia, D., Wasowski, J., Santaloia, F., & Lollino, P. (2022). Regional-Scale Seismic Liquefaction Susceptibility Mapping via an Empirical Approach Validated by Site-Specific Analyses. Geosciences, 12(5), 215. https://doi.org/10.3390/geosciences12050215

© 2026 Journal of Geoscience, Engineering, Environment and Technology. All rights reserved. This is an open access article distributed under the terms of the CC BY-SA License (http://creativecommons.org/licenses/by-sa/4.0/).